Chinese Journal of Chemical Engineering 27 (2019) 965–978

Contents lists available at ScienceDirect

Chinese Journal of Chemical Engineering

journal homepage: www.elsevier.com/locate/CJChE

Article

Synthesis, characterization and electrochemical evaluation of anticorrosion property of a tetrapolymer for carbon steel in strong acid media

Shamsuddeen A. Haladu [1], Saviour A. Umoren [2,*], Shaikh A. Ali [3], Moses M. Solomon [2], Abdul-Rashid I. Mohammed [4]

[1] Department Basic Sciences and Humanities, College of Engineering, Imam Abdulrahman Bin Faisal University, Dammam 31451, Saudi Arabia
[2] Centre of Research Excellence in Corrosion, Research Institute, King Fahd University of Petroleum and Minerals, Dhahran 31261, Saudi Arabia
[3] Department of Chemistry, King Fahd University of Petroleum & Minerals, Dhahran 31261, Saudi Arabia
[4] Centre for Engineering Research, Research Institute, King Fahd University of Petroleum and Minerals, Dhahran 31261, Saudi Arabia

ARTICLE INFO

Article history:
Received 15 May 2018
Received in revised form 4 July 2018
Accepted 19 July 2018
Available online 1 August 2018

Keywords:
Tetrapolymer
Metal
Acid corrosion
Corrosion inhibition
Adsorption
Synergism

ABSTRACT

A novel tetrapolymer (TP) consisting of carboxylate, sulphonate, phosphonate and sulfur dioxide based co-monomers was synthesized using Butler cyclopoymerization technique. The synthesized tetrapolymer was characterized using FTIR, ^{1}H-NMR, ^{13}C NMR and elemental analysis. The performance of the tetrapolymer as a corrosion inhibitor for St37 carbon steel in 15% HCl and 15% H_2SO_4 acid media was assessed using electrochemical impedance spectroscopy (EIS), linear polarization resistance (LPR), potentiodynamic polarization (PDP) and electrochemical frequency modulation (EFM) techniques. The influence of addition of a small amount of KI on the corrosion inhibition efficiency of TP was also assessed. Results obtained showed that the tetrapolymer moderately inhibited the corrosion of St37 steel in the acid media with protection efficiency of 79.5% and 61.1% at the optimum concentration of 1000 mg·L^{-1} studied in HCl and H_2SO_4 media respectively. On addition of 5 mmol·L^{-1} KI to the optimum tetrapolymer concentration, the protection efficiency was upgraded to 90.6% and 93.5% in HCl and H_2SO_4 environment, respectively. The enhanced performance of the polymer in the presence of KI is due to synergistic action deduced from synergism parameter (S_1) which was found to be greater than unity. The tetrapolymer afforded the corrosion inhibition of St37 steel in the acid media by virtue of adsorption of the polymer molecules on the steel surface which was confirmed by ATR-FTIR analysis of the adsorbed film extracted from the steel surface. TP + KI formed complex with St37 steel surface in H_2SO_4 solution but not in HCl solution.

1. Introduction

In the process of acidizing stimulation or cleanup operations, metal tubulars, down hole tools/valves, surface lines, *etc.* mainly made of carbon steel are exposed to acidic fluids [1]. The exposure is detrimental to the carbon steel materials as they are prone to corrosion. In addition, metal substrates in high temperature wells experience a drastic increase in corrosion rates. Therefore, controlling corrosion is critical and must be dealt with effectively. In addition, corrosion protection becomes inevitable in order to maintain the integrity and long life of down hole tools installed in an operating oil wells.

Although there are many corrosion protection strategies adopted to control corrosion of metal substrates in diverse corrosive media, the use of corrosion inhibitors for internal pipeline corrosion protection offers the most practical and cost effective method. The key performance indicators for the selection of corrosion inhibitor include its economic availability, performance (effectiveness to inhibit the metal substrate) and its environmental side effects. Most of the inhibitors for corrosion of steel in acidic media are organic compounds containing nitrogen, oxygen and/or sulfur atoms. The inhibiting action of these compounds is often associated with their ability to adsorb on the metal/solution interface. The use of polymers and polymer composites as corrosion inhibitor for steel in strong acid media can be found in the literature [2–7]. In our laboratory, we have also reported on the use of cyclic cation polymer bearing bis-3-phosphorylpropyl pendants [8] and polypropylene glycol [9] as effective corrosion inhibitors for steel in 15% HCl medium.

Apart from corrosion, there are other problems in the oil and gas industry that required the use of specialty chemicals for treatment. For instance, antiscalants or scale inhibitors are required for scale inhibition, biocides to inhibit the growth of microorganisms/biofouling and demulsifiers or emulsion breakers to separate emulsions, for example water in oil. The use of diverse chemicals simultaneously to treat different problems occurring in the oil field sometimes results in

* Corresponding author.
E-mail address: umoren@kfupm.edu.sa (S.A. Umoren).

https://doi.org/10.1016/j.cjche.2018.07.015
1004-9541/

the problem of incompatibility. It is highly desirable to have a single compound with dual or multi multi functions. Previous work has shown that the tetrapolymer acted as an effective antiscalant for $CaSO_4$ scale [10]. In order to explore the possibility of tetrapolymer serving a dual purpose as a scale inhibitor and as well as a corrosion inhibitor, the present work reports on the corrosion inhibition performance of tetrapolymer for carbon steel (St37 grade) in 15% HCl and 15% H_2SO_4 environments using electrochemical techniques. The effect of the addition of KI on the corrosion inhibition performance of the investigated tetrapolymer was also assessed. Analysis of the adsorbed inhibitor film on the steel surface in comparison with that of the bulk polymer using ATR-FTIR technique was employed to elucidate the mechanism of corrosion inhibition by the tetrapolymer.

2. Experimental

2.1. Synthesis and characterization of tetrapolymer

The details of the synthesis of the tetrapolymer using Butler cyclopolymerization technique. The polymerization was carried out in a solution of **1** (2.75 g, 15 mmol), **2** (3.83 g, 15 mmol), and **3** (3.29 g, 15 mmol) SO_2 (2.88 g, 45 mmol) in DMSO (12.5 g) using azobisobutyronitrile (AIBN) (225 mg) (Scheme 1). The mixture was stirred under N_2 in a closed RB flask at 60 °C for 48 h. Every 8 h, the flask was opened to release N_2 generated from the decomposition of AIBN. The reaction mixture became immobile within an hour; at the end of the time elapsed, the reaction mixture was soaked in water, filtered and washed with acetone. The white polymer **4** was then grounded with a mortar and pestle and soaked in methanol, filtered, and dried under vacuum at 60 °C to a constant weight (11.0 g, 90%). The characterization of the obtained tetrapolymer was done using FTIR, ^{13}C NMR, ^{1}H NMR, and elemental analysis. The results from FTIR, ^{13}C NMR, and elemental analysis can be found in reference [10]. Only ^{1}H NMR spectrum is presented herein.

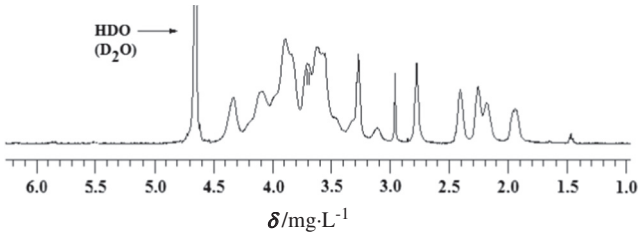

Fig. 1. ^{1}H NMR spectrum of tetrapolymer **4** in D_2O in the presence of NaCl.

2.2. Corrosion inhibition studies

2.2.1. Materials and corrosive media

St37 steel with chemical composition as earlier reported [11] was used as the metal substrate. The corrosive media was 15% HCl and 15% H_2SO_4 prepared by diluting analytical reagent grade 37% HCl (Sigma Aldrich) and 98% H_2SO_4 (Sigma-Aldrich) with doubled distilled water. The synthesized polymer was used as test corrosion inhibitor in the concentration range of 50–1000 mg·L^{-1}. KI (Sigma Aldrich) concentration of 1 mmol·L^{-1} and 5 mmol·L^{-1} was added to 1000 mg·L^{-1} of TP to evaluate the synergistic effect of KI additive.

2.2.2. Electrochemical corrosion tests

Electrochemical corrosion tests were conducted using the Gamry Potentiostat/Galvanostat/ZRA Reference 600 together with Echem analyst software to analyze the experimental data. Conventional three electrode assembly was used to accomplish the electrochemical measurements. The electrodes were made up of St37 steel as working, silver/silver chloride (Ag/AgCl) as reference and graphite rod as the counter electrodes. The working electrode was in the form of a circular disc with an exposed surface area of 0.75 cm^2. Prior to all electrochemical measurements, the working electrode was immersed for 1 h to ensure that the steady-state open circuit potential (OCP) was established. Potentiodynamic polarization tests were performed at the potential of ±150 mV from open circuit potential (OCP) at a scan rate of 0.5 mV·s^{-1}. LPR experiment was carried out from −15 to +15 mV *versus* OCP at the scan rate of 0.125 mV·s^{-1}. Electrochemical impedance spectroscopy (EIS) tests were monitored over the frequency range of 10^4 to 10 mHz, with acquirement of 10 points per decade and a signal amplitude of 10 mV (peak-to-peak) at E_{corr}. EFM measurements were carried using potential perturbation signal with amplitudes of 10 mV. Measurements were conducted using two frequencies, 2 and 5 Hz. The base frequency was 1 Hz with 32 cycles so the waveform repeats after 1 s. All measurements were repeated at least three times and good reproducibility of the results was observed.

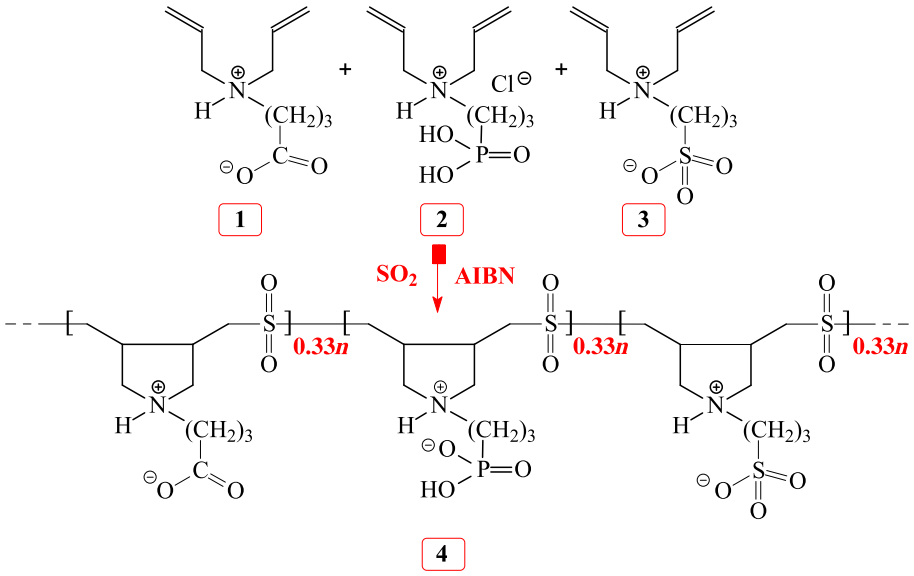

Scheme 1. Synthesis of the tetrapolymer **4**.

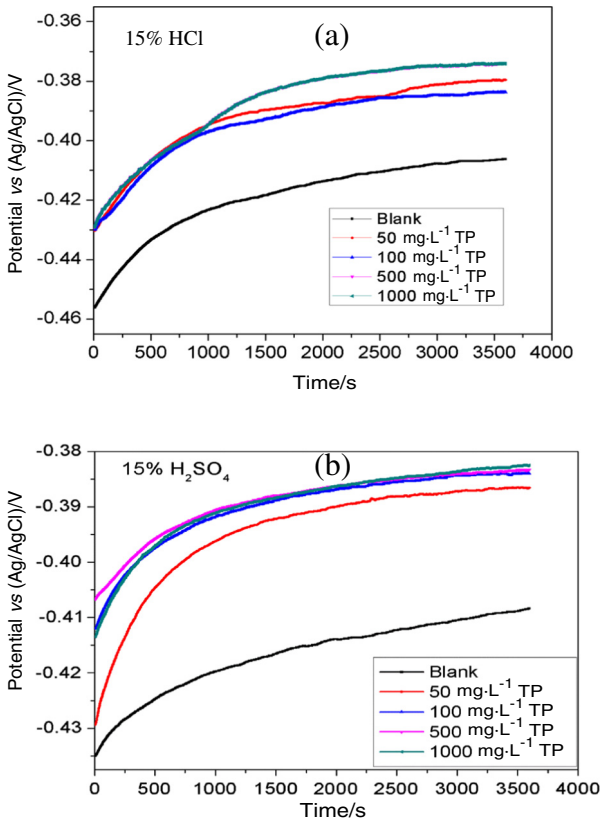

Fig. 2. Variation of OCP with time for St37 steel in (a) 15% H_2SO_4 and (b) 15% HCl in the absence and presence of different concentrations of TP at 25 °C.

2.2.3. Surface analysis

The morphology of the corroded steel surfaces immersed in the corrosive medium in absence and presence of TP and TP in combination of KI were determined using scanning electron microscope (SEM) (JEOL JSM 6610-LV) operated at an acceleration voltage of 20 kV and irradiation current of 10 μA.

The UV–Visible spectra were recorded for solutions of 15% HCl and 15% H_2SO_4 devoid of and containing TP and TP–KI mixtures after 24 h immersion of the carbon steel using JASCO770-UV–Vis spectrophotometer from 250 to 450 nm using a dual beam operated at a resolution of 1 nm with a scan rate of 200 nm·min^{-1}.

The ATR-FTIR analysis was performed for pure TP and the films extracted from the carbon steel surface immersed in 15% HCl and 15% H_2SO_4 containing TP and TP–KI mixtures for 24 h at 25 °C. The ATR-FTIR spectra were recorded in the range of 400–4000 cm^{-1} using an IR spectrometry (TA instrument with universal ATR attachment, Nicolet iS5, Thermo Scientific).

3. Results and Discussion

3.1. Characterization of tetrapolymer (TP)

The ^{1}H NMR spectrum in D_2O (Fig. 1) revealed the formation of the polymer as indicated by the absence of alkene-proton signals of **1–3** which should appear between δ value of 5.5–6.0 mg·L^{-1}.

3.2. Corrosion inhibition by TP

The corrosion inhibition ability of TP for St37 corrosion in strong acid environments was assessed using electrochemical approaches. For results obtained from electrochemical experiments to be valid, the essential requirements of linearity, causality, and stability must be met [12]. Fig. 2 shows the variation of OCP of St37 steel with time in (a) 15% HCl and (b) 15% H_2SO_4 solutions without and with various concentrations of TP at ambient temperature (25 °C). Although there is a slight difference in the length of time taken for a steady state condition to be attained in the various systems, it is obvious that a quasi-steady-state was achieved in all cases within the 3600 s waiting time hence the electrochemical results presented herein should be valid. In the HCl (Fig. 2(a)) and H_2SO_4 (Fig. 2(b)) solutions devoid of TP, the initial OCP values of the specimen are –456 mV/Ag/AgCl and – 440 mV/Ag/AgCl respectively. The presence of TP in these media caused noticeable potential shift towards nobler OCP values indicating the appearance of TP adsorbed layer on the steel surface [13,14].

In Fig. 3 is presented the potentiodynamic polarization curves obtained for St37 steel electrode in (a) 15% HCl and (b) 15% H_2SO_4 solutions devoid of and containing various concentrations of TP at ordinary temperature. The relevant electrochemical polarization parameters namely, corrosion potential (E_{corr}), corrosion current density (I_{corr}), and the anodic and cathodic slopes (β_a, β_c) deduced from the graphs are given in Table 1. Also displayed in Table 1 are the polarization resistance (R_p) and corrosion rate (CR) obtained from linear polarization graphs (not shown). The extent of corrosion inhibition (IE) by TP from potentiodynamic polarization and linear

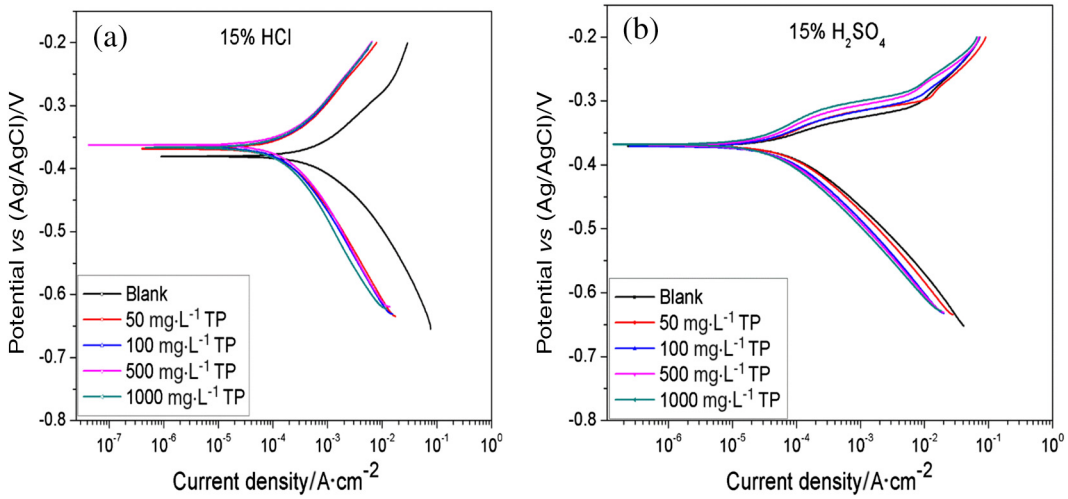

Fig. 3. Potentiodynamic polarization curves for St37 steel in (a) 15% H_2SO_4 and (b) 15% HCl in the absence and presence of different concentrations TP at 25 °C.

Table 1
Potentiodynamic polarization (PDP) and Linear polarization resistance (LPR) parameters for St37 steel in 15% HCl and 15% H_2SO_4 without and with different concentrations of TP at 25 °C.

Medium	Concentration/mg·L^{-1}	PDP method					LPR method		
		E_{corr} (Ag/AgCl)/mV	I_{corr}/μA·cm^{-2}	β_a/mV·dec^{-1}	β_c/mV·dec^{-1}	*IE*/%	R_p/Ω·cm^{-2}	*CR*/mpy	*IE*/%
15% H_2SO_4	Blank	−371	63.5	48.6	81.6	–	132.0	120.2	–
	50	−370	56.4	63.4	74.1	11.2	212.0	74.7	37.7
	100	−371	44.0	59.9	74.4	30.7	280.0	56.7	52.9
	500	−370	41.1	70.4	77.5	35.3	318.9	49.8	58.6
	1000	−368	35.2	72.0	79.4	44.6	363.0	43.7	63.6
15% HCl	Blank	−381	649.0	87.6	89.5	–	35.6	445.8	–
	50	−368	211.0	107.6	148.3	67.5	67.5	235.2	47.2
	100	−366	191.0	101.5	131.8	70.6	86.3	183.3	58.8
	500	−362	188.0	104.0	167.4	71.0	120.5	131.7	70.5
	1000	−367	183.0	93.4	130.0	71.8	159.1	99.8	77.6

Note: 1mpy=0.0254mm·a^{-1}.

polarization techniques was computed making use of the I_{corr} and R_p values respectively according to the following equations:

$$IE = \frac{I_{corr(blank)} - I_{corr(TP)}}{I_{corr(blank)}} \times 100\% \quad (1)$$

$$IE = \frac{R_{p(TP)} - R_{p(blank)}}{R_{p(TP)}} \times 100\% \quad (2)$$

From Fig. 3, it is observed that addition of TP to the corrosive media has minimal influence on E_{corr}, *i.e.* the corrosion potential is only shifted slightly towards anodic direction. Both the oxidative dissolution of St37 steel electrode in the anodic region and the hydrogen reduction in the cathodic region are suppressed. These observations are common with mixed type corrosion inhibitors [15,16]. The changes in both β_a and β_c values relative to those of the blank (Table 1) also point to the mixed type behavior of TP in the studied environments [15,16]. A quick comparison of Fig. 3(a) to (b) reveals that TP is a better corrosion inhibitor for St37 steel in HCl environment than in H_2SO_4 medium. As could be seen in the figure and in Table 1, there is a remarkable reduction in I_{corr} by TP relative to the blank in HCl solution than in H_2SO_4 solution. For instance, in H_2SO_4 solution, the addition of 1000 ppm TP resulted in a decline in I_{corr} value from 63.5 μA·cm^{-2} to 35.2 μA·cm^{-2} and the calculated *IE* is 44.6%. The addition of the same concentration of TP to 15% HCl solution caused a decrease in I_{corr} value from 649.0 μA·cm^{-2} to 183.0 μA·cm^{-2} with 71.8% as the *IE*. This seems to suggest that the anions (chlorides in HCl and sulphates in H_2SO_4) played a vital role in the adsorption process of TP onto the steel surface. It is also observed from the table that the I_{corr} and *CR* values decrease while R_p and *IE* values increase with increasing TP concentration. This could mean availability of more inhibitor molecules for adsorption as the concentration increases.

Fig. 4 shows the electrochemical impedance spectroscopy (EIS) results obtained for ST37 steel in free 15% HCl and 15% H_2SO_4 solutions

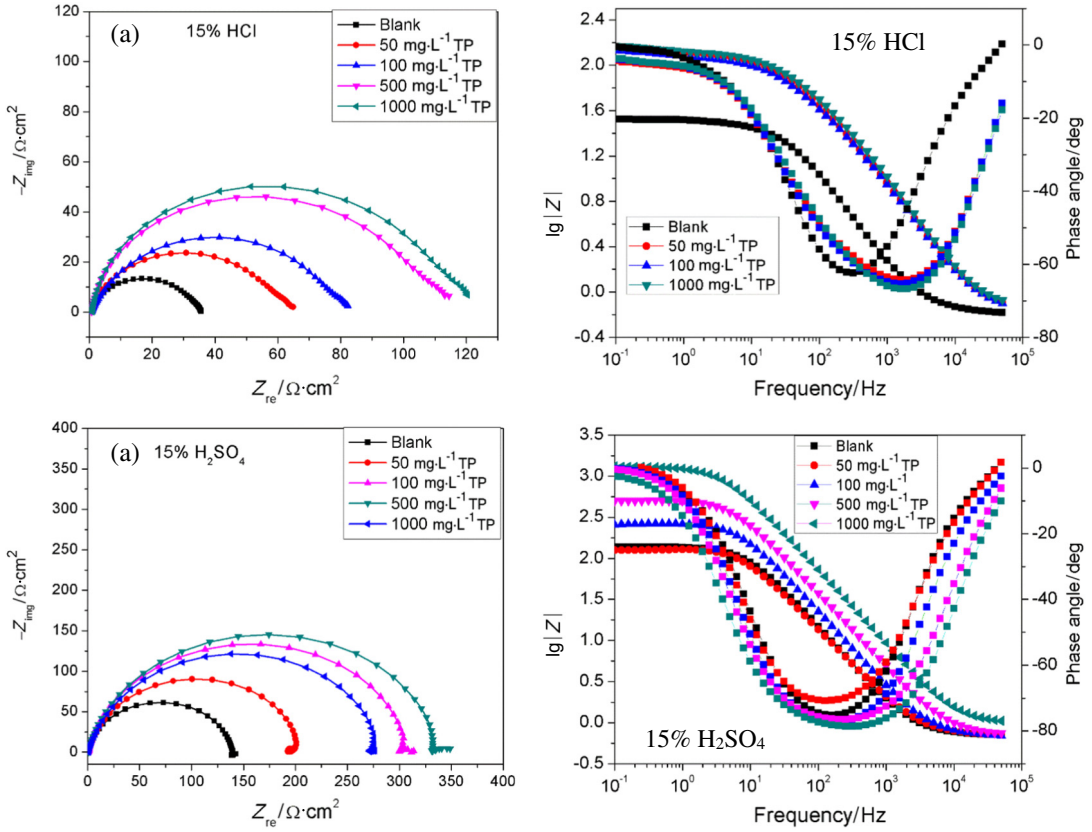

Fig. 4. EIS plots for St37 steel in 15% H_2SO_4 and 15% HCl in the absence and presence of different concentrations of TP at 25 °C in (a) Nyquist and (b) Bode representations.

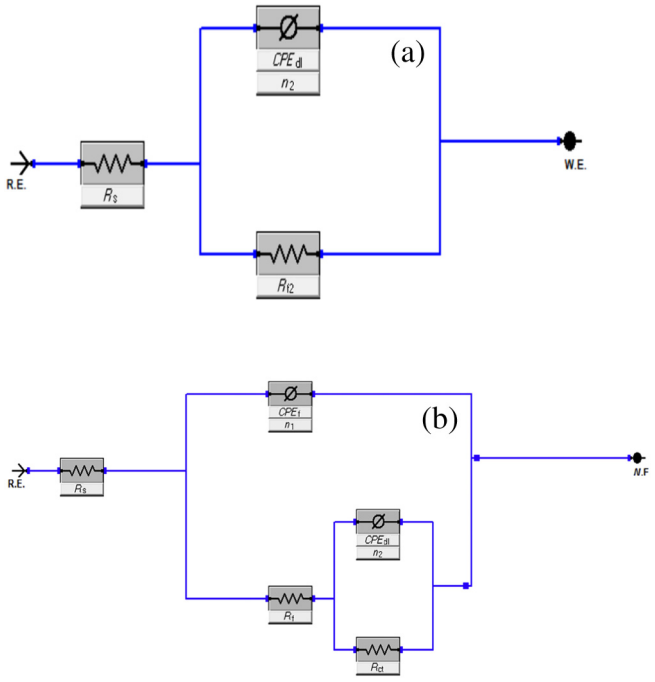

Fig. 5. Equivalent circuit diagrams used to fit impedance data in the (a) blank and (b) presence of TP.

and in the acid solutions fortified with various concentrations of TP in different formats namely (a, c) Nyquist and (b, d) Bode and Phase angle. In the Nyquist diagrams recorded in the free acid solutions, single capacitive loops often linked to charge transfer corrosion process are observed in the high frequencies and they correspond to one time constant in the Bode and Phase angle representations. In the case of TP inhibited systems, two capacitive loops corresponding to two time constants in Fig. 4 (b, d) at the high and medium frequencies can be identified. The two time constants could arise from the double layer structure of the TP adsorbed film on the steel surface [17–19]. To this end, a simple RQR equivalent circuit (Fig. 5(a)) was used for the fitting of the Nyquist curves recorded in the uninhibited systems while the RQ(RQR) equivalent circuit (Fig. 5(b)) was deployed for the analysis of the Nyquist graphs obtained in the TP inhibited acid solutions.

The quite small chi-square values (in the range 19.4×10^{-5} – 82.4×10^{-5}) (Table 2) and the low values of fitting errors associated with the parameters (less than 5% in all cases) suggested the fitted results were reliable. Accordingly, the physical meanings of the elements in Fig. 5(b) are as follow; R_s represents the solution resistance, R_{f1} and CPE_f stand for the resistance and constant phase element of the outer layer of the adsorbed TP film respectively, R_{f2} and CPE_{dl} denote the resistance and constant phase element of the inner layer of the adsorbed inhibitor film respectively [18,19]. The use of *CPE* was essential for good quality fit owing to the imperfectness of the capacitive loops [19]. The performance of adsorbed inhibitor film can be judged from the polarization resistance (R_p) since inhibition efficiency varies directly with film corrosion resistance [19]. The parameter R_p is defined as $R_p = (Z_F)\omega = 0$ [18,19], where Z_F = faradaic impedance of circuit and ω = angular frequency. According to Wang *et al.* [19], R_p can be expressed as the summation of the resistances of the outer and inner film layers (*i.e* $R_p = R_{f1} + R_{f2}$). For the uninhibited system, $R_p = R_{f2}$. Therefore, the corrosion protection performance of the TP adsorbed film was evaluated making use of R_p values according to the following equation:

$$IE = \frac{R_{p(\text{inhibited})} - R_{p(\text{uninhibited})}}{R_{p(\text{inhibited})}} \times 100\% \quad (3)$$

The values of all the parameters associated with the evaluated systems from this technique are displayed in Table 2. From the table, it can be deduced that charge transfer process was difficult in the inhibited systems compared to the uninhibited and this phenomenon may have been caused by the adsorption of TP molecules onto the St37 electrode surface in the inhibited systems. The influence of increase in TP concentration on the R_{f2} and R_p of the adsorbed film is obvious in Table 2 and Fig. 4. For instance, the diameter of the Nyquist graphs (Fig. 4(a, c)), impedance and phase angle (Fig. 4(b, d)), the R_{f2} and R_p values increased with increasing TP concentration. Increase in inhibitor concentration may have resulted in larger surface coverage. Interestingly, the values of R_{f1} is found to increase with increase in TP concentration in H_2SO_4 systems but decreases in HCl systems yet the inhibitor performed better in HCl medium than in H_2SO_4 solution. This may reflect the dependency of corrosion protection ability of adsorbed film on the resistive strength of the inner layer than the outer layer. Based on the values of n_1 and n_2 (Table 2) which are near unity, it is concluded that the interface behaved nearly capacitive since $n = 0$ represents a pure resistor, $n = -1$ infers inductor, and $n = +1$ denotes a pure capacitor [7,11].

To further confirm the corrosion inhibition effect of TP on St37 steel in the considered acid solutions, electrochemical frequency modulation (EFM) was undertaken. The beauty of EFM lies on the inherent data validation control through the use of causality factors (*CF*-2 and *CF*-3). As a rule, EFM results are adjudged valid only when the values of *CF*-2 and *CF*-3 are within the range 0–2 and 0–3 respectively [4,20]. The representative EFM spectra for ST37 electrodes in the studied media are shown in Fig. 6. Two sets of peaks characterized the spectra — intense and clouded peaks. The intense peaks represent the harmonic and intermodulation signals while the clouded bands represent the background noise signals [4,21]. Only the harmonic and intermodulation peaks were therefore selected for the computation of the corrosion parameters listed in Table 3. The values of I_{corr} and *CR* in the table vary in similar manner as those in Table 1 with TP concentration. Again, both β_a

Table 2
Impedance parameters for St37 steel in 15% HCl and 15% H_2SO_4 without and with different concentrations of TP at 25 °C

Medium	Concentration/mg·L^{-1}	R_s/Ω·cm^{-2}	CPE_f			CPE_{dl}			R_p/Ω·cm^{-2}	$\chi^2 \times 10^{-5}$	*IE*/%
			Y_{o1}/μΩ·s^n·cm^{-2}	n_1	R_{f1}/Ω·cm^{-2}	Y_{o2}/μΩ·s^n·cm^{-2}	n_2	R_{f2}/Ω·cm^{-2}			
15% H_2SO_4	Blank	0.74	–	–	–	141.7	0.93	129.6	129.6	20.9	–
	50	0.65	124.3	0.91	61.3	6240	0.99	138.1	199.4	50.	35.0
	100	0.81	89.7	0.91	79.8	21.2	0.94	196.4	276.2	27.9	53.1
	500	0.76	69.7	0.93	135.2	4016	0.88	169.5	304.7	26.9	57.4
	1000	0.77	68.2	0.92	156.7	560.7	0.87	176.7	333.4	19.4	61.1
15% HCl	Blank	0.65	–	–	–	328.3	0.86	32.1	32.1	56.8	–
	50	0.70	201.7	0.84	4.2	1361.0	0.96	60.3	64.5	43.9	50.2
	100	0.69	242.7	0.80	39.5	1687.0	0.99	40.7	80.2	33.8	59.9
	500	0.79	238.2	0.93	13.2	851.3	0.79	103.7	116.9	66.2	72.5
	1000	0.75	32.8	0.90	4.1	851.3	0.93	152.3	156.4	82.4	79.5

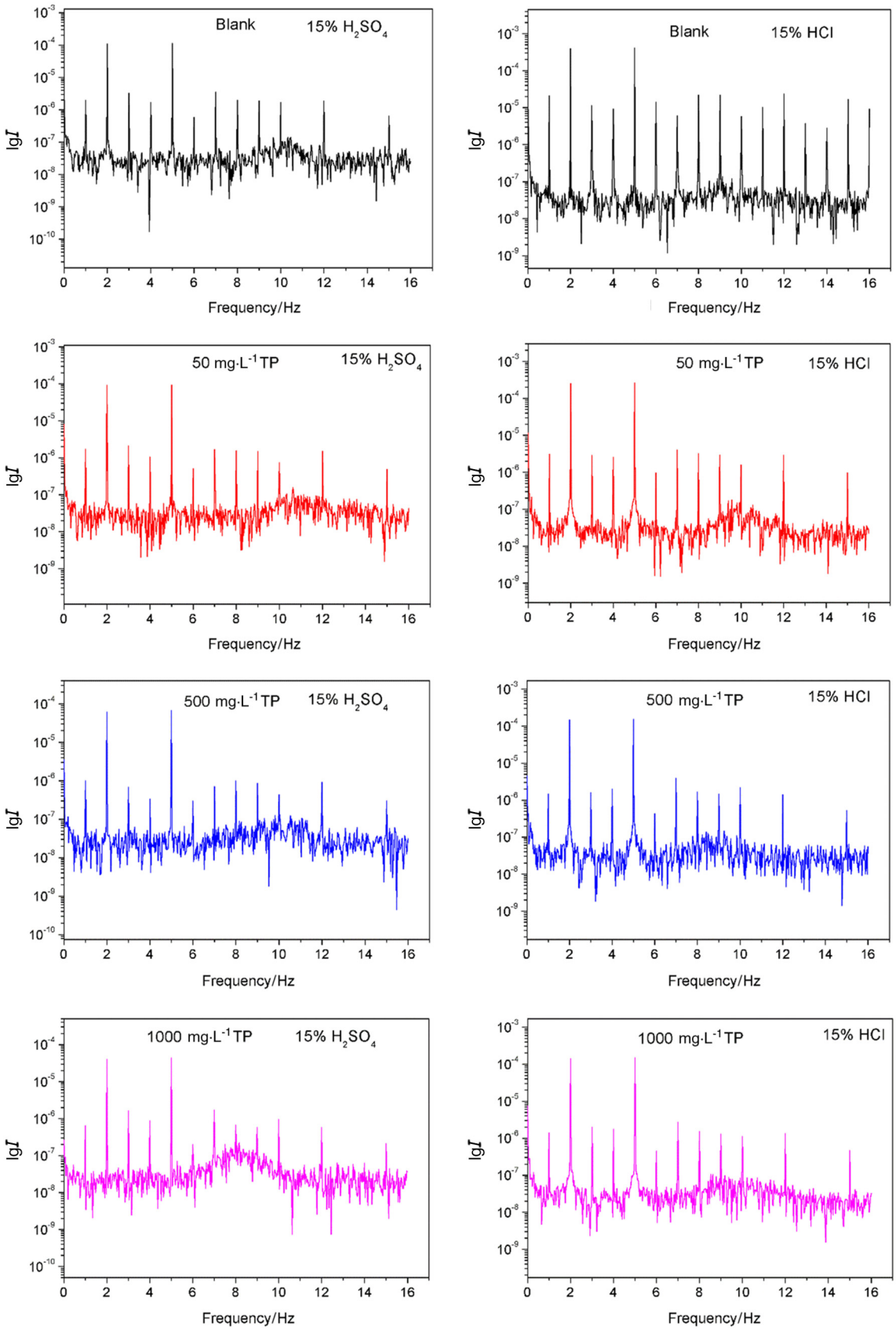

Fig. 6. Intermodulation spectrum recorded for St37 steel in 15% HCl solution in absence and presence of different concentrations of TP at 25 °C.

Table 3
Electrochemical frequency modulation parameters for St37 steel in 15% HCl and 15% H_2SO_4 in the absence and presence of different concentrations of TP at 25 °C

Medium	Concentration/mg·L^{-1}	I_{corr}/μA·cm^{-2}	β_a/mV·dec^{-1}	β_c/mV·dec^{-1}	*CR*/mpy	*CF*-2	*CF*-3	*IE*/%
15% H_2SO_4	Blank	150.1	81.4	96.1	91.4	2.00	3.06	–
	50	112.3	88.2	107.8	68.4	1.92	3.13	25.2
	100	82.5	90.7	105.9	50.2	1.82	3.17	45.0
	500	72.1	87.8	121.1	43.9	1.85	2.86	51.9
	1000	62.7	87.0	110.7	38.2	1.45	2.98	58.2
15% HCl	Blank	928.0	95.9	105.7	533.7	1.69	3.13	–
	50	412.4	101.6	111.4	251.3	1.62	3.13	55.6
	100	334.2	102.3	111.8	203.6	1.54	3.16	63.9
	500	286.8	127.1	138.1	175.9	1.39	3.14	69.1
	1000	264.0	111.5	125.3	160.8	1.64	3.06	71.6

and β_c values are affected with increasing TP concentration supporting the mixed type behavior of TP earlier proposed. The *CF*-2 and *CF*-3 values are within the acceptable limits and thus valid the obtained EFM results. There is good agreement between the *IE* values obtained from this technique with those from other electrochemical techniques (Tables 1 & 2).

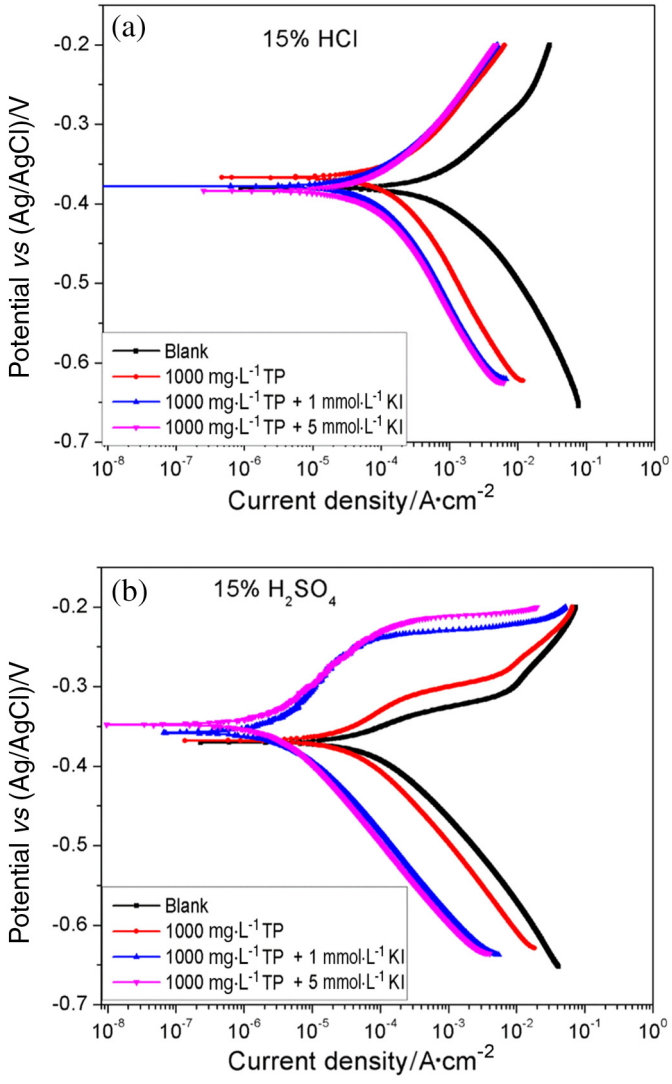

Fig. 7. Potentiodynamic polarization curves for St37 steel in (a) 15% H_2SO_4 and (b) 15% HCl in the absence and presence of TP (1000 mg·L^{-1}) and TP + KI mixtures at 25 °C.

3.3. Effect of KI on TP performance

In a couple of our previous reports [22–24], we had demonstrated the enhanced corrosion inhibition of polymers by iodide ions due to their strong chemisorption ability. In this present work, it was reasonable to attempt a strategy through which the corrosion inhibition strength of TP can be improved owing to the fact that, the optimum concentration of the polymer (1000 mg·L^{-1}) could only afford 55.5% and 63.4% corrosion inhibition to St37 steel in 15% HCl and 15% H_2SO_4 media respectively. In this regard, we added small amounts (1 mmol·L^{-1} and 5 mmol·L^{-1}) of KI to the optimum concentration of TP and the effect of this addition on the inhibition efficiency was studied using PDP, LPR, EIS, and EFM. Fig. 7 shows the comparative PDP graphs of St37 steel in (a) 15% HCl and (b) 15% H_2SO_4 solutions without and containing 1000 mg·L^{-1} TP, 1000 mg·L^{-1} TP + 1 mmol·L^{-1} KI, and 1000 mg·L^{-1} TP + 5 mmol·L^{-1} KI respectively. All the polarization parameters derived from the graphs are given in Table 4. Obviously, the addition of iodide ions to TP was a beneficial strategy. In Fig. 7 and Table 4, it is very clear that the addition of KI to TP resulted in significant reduction in the corrosion current densities than that of TP alone. This reduction manifested in higher corrosion protection. For instance, on addition of 1 mmol·L^{-1} KI and 5 mmol·L^{-1} KI to 1000 mg·L^{-1} TP, the I_{corr} values of 35.2 μA·cm^{-2} and 183.0 μA·cm^{-2} for TP alone in H_2SO_4 and HCl solutions respectively were drastically reduced to 4.1 μA·cm^{-2} and 2.9 μA·cm^{-2} in H_2SO_4 medium and 78.3 μA·cm^{-2} and 76.4 μA·cm^{-2} in HCl solution. The inhibition efficiency was upgraded from 44.8% in H_2SO_4 solution to 93.5% and 95.4% on addition of 1 mmol·L^{-1} KI and 5 mmol·L^{-1} KI respectively. Similarly, the *IE* of TP in HCl was raised from 71.8% to 87.9% and 88.2% by the addition of 1 mmol·L^{-1} KI and 5 mmol·L^{-1} KI respectively. This is a clear indication that the TP + KI adsorbed protective film covered greater surface area than TP adsorbed film and probably were more stable. A close inspection of Fig. 7(a) reveals that TP + KI mixture suppressed cathodic reactions more than the anodic reactions. In the anodic branches of the TP + KI graphs in Fig. 7(b), at corrosion potential nobler than – 250 mV/(Ag/AgCl), the inhibition effect of the mixture seems to decline and remain near constant for a wide range of potential. For instance, the graphs appear somewhat parallel to the *x*-axis. Qian *et al.* [25] had reported similar observation and was interpreted to mean desorption potential where the desorption rate of the adsorbed film is higher than the adsorption rate. By comparing the *IE* values of TP + KI in HCl systems to those in H_2SO_4 solutions (Table 4), it is found that the values are higher in H_2SO_4 than HCl which is a reverse of what was observed in the case of TP alone (Tables 1–3). The possible cause of this reversal is explained in Section 3.6. In Table 4 is also presented the R_p, *CR*, and *IE* values obtained from LPR measurements for the studied substrate and systems. In both acid media, the polarization and corrosion rate of the substrate are greatly reduced by TP + KI mixture but the effect is more in H_2SO_4 medium than HCl and thus agree with the PDP findings. *IE* of 94.9% and 95.8% are obtained from this technique for TP + 1 mmol·L^{-1} KI

Table 4
Potentiodynamic polarization (PDP) and Linear polarization resistance (LPR) parameters for St37 steel in 15% HCl and 15% H_2SO_4 without, with 1000 mg/L TP, KI and TP + KI mixtures at 25 °C.

Medium	Concentration	PDP method					LPR method		
		E_{corr} (Ag/AgCl)/mV	I_{corr}/μA·cm^{-2}	β_a/mV·dec^{-1}	β_c/mV·dec^{-1}	*IE*/%	R_p/Ω·cm^2	*CR*/mpy	*IE*/%
15% H_2SO_4	Blank	−371	63.5	48.6	81.6	–	132.0	120.2	–
	TP (1000 mg·L^{-1})	−368	35.2	72.0	79.4	44.8	363.0	43.7	63.4
	1 mmol·L^{-1} KI	−363	4.3	120.6	85.4	93.2	1811	8.8	92.7
	5 mmol·L^{-1} KI	−347	3.8	127.1	115.4	94.0	2143	7.4	93.8
	TP + 1 mmol·L^{-1} KI	−358	4.1	126.4	79.7	93.5	2593	6.1	94.9
	TP + 5 mmol·L^{-1} KI	−348	2.9	82.3	96.9	95.4	3158	5.0	95.8
15% HCl	Blank	−381	649.0	87.6	89.5	–	35.6	445.8	–
	TP (1000 mg·L^{-1})	−367	183.0	104.0	167.4	71.8	159.1	99.8	77.6
	1 mmol·L^{-1} KI	−386	218.0	77.6	91.2	66.4	80.0	198.4	55.5
	5 mmol·L^{-1} KI	−397	158.0	80.4	108.7	75.7	116.2	136.6	69.4
	TP + 1 mmol·L^{-1} KI	−378	78.3	82.0	120.0	87.9	313.8	50.58	88.7
	TP + 5 mmol·L^{-1} KI	−384	76.4	84.7	125.1	88.2	331.8	47.8	89.3

and TP + 5 mmol·L^{-1} KI respectively in H_2SO_4 solution while the values are 88.7% and 89.3% in HCl environment.

The Nyquist, Bode, and Phase angle plots for St37 steel in (a, b) 15% HCl and (c, d) 15% H_2SO_4 solutions without and with additives are shown in Fig. 8. The equivalent circuit in Fig. 5(b) was used for the analysis of the TP + KI Nyquist graphs. All the parameters pertaining to these systems are given in Table 5. As could be seen in Fig. 8(a, c), the semicircles at high frequencies in the TP + KI Nyquist graphs are outstandingly larger than those of TP alone and the second loop in the medium frequencies becomes very pronounced. There is also a noticeable displacement in the impedance and phase angle in Fig. 8(b, d) on the addition of KI to TP. All these indicate the enhancement in corrosion inhibition efficiency of TP by KI. The results in Table 5 reveals that the polarization resistance of St37 steel in the acid solutions was increased by a factor of more than 10 on the introduction of KI into the corrosive systems containing 1000 mg·L^{-1} TP. It can be concluded from the results in Table 5 that in 15% H_2SO_4 environment, ST37 steel surface can be protected against corrosion by 93.4% and 93.5% while in 15% HCl, corrosion protection of 79.5% and 89.7% can be achieved on the addition of 1 mM KI and 5 mM KI respectively to 1000 mg·L^{-1} TP.

Fig. 9 shows the EFM spectra recorded for St37 steel in strong acid media without and with various additives as corrosion inhibitor and the parameters deduced from the analysis of the spectra are presented in Table 6. The obtained *CF*-2 and *CF*-3 values are within the acceptable limit and the I_{corr} values are in perfect agreement with those derived from PDP experiments. There is also clear evidence of improved TP corrosion inhibition efficiency by KI addition. The *IE* values from all the electrochemical techniques are in good agreement and point to synergistic corrosion inhibition between TP and iodide ions. To determine whether the observed improvement in the corrosion inhibition efficiency of TP upon combination with iodide ions is due to synergistic effect, we calculated the synergism parameter (S_1). As it is known,

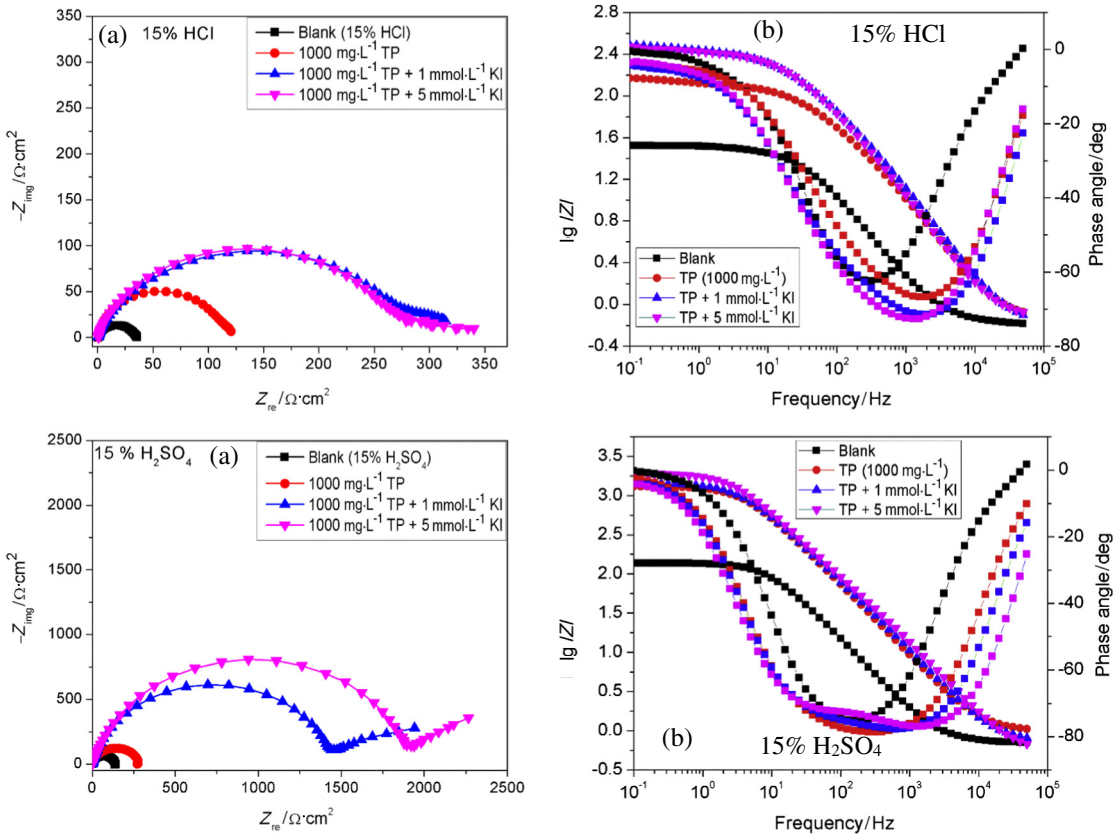

Fig. 8. EIS plots for St37 steel in 15% H_2SO_4 and 15% HCl in the absence and presence of TP (1000 mg·L^{-1}) and TP + KI mixtures at 25 °C in (a) Nyquist and (b) Bode representations.

Table 5
Impedance parameters for St37 steel in 15% HCl and 15% H_2SO_4 without, with 1000 mg·L^{-1} TP and TP + KI mixtures at 25 °C

Medium	Concentration	CPE_f			CPE_{dl}			$R_{ct}/\Omega\cdot cm^{-2}$	$R_p/\Omega\cdot cm^{-2}$	$\chi^2\times10^{-5}$	$IE/\%$
		$R_s/\Omega\cdot cm^{-2}$	$Y_{o1}/\mu\Omega\cdot s^n\cdot cm^{-2}$	n_1	$R_f/\Omega\cdot cm^{-2}$	$Y_{o2}/\mu\Omega\cdot s^n\cdot cm^{-2}$	n_2				
15% H_2SO_4	Blank	0.74	–	–	–	141.7	0.93	129.6	129.6	20.9	–
	TP (1000 mg·L^{-1})	0.77	68.2	0.92	156.7	40.9	0.87	176.7	333.4	19.4	61.1
	1 mmol·L^{-1} KI	0.74	71.4	0.89	263.2	54.2	0.99	1052.0	1315.2	86.3	90.1
	5 mmol·L^{-1} KI	0.76	67.4	0.88	302.9	52,450	0.99	1362.0	1664.9	124.9	92.2
	TP + 1 mmol·L^{-1} KI	0.71	39.8	0.90	506.5	17,060	0.96	1456.0	1962.5	146.6	93.4
	TP + 5 mmol·L^{-1} KI	0.60	15.9	0.96	81.2	29.9	0.78	1923.0	2004.2	204.6	93.5
15% HCl	Blank	0.65	–	–	–	328.3	0.86	32.1	32.1	56.8	–
	TP (1000 mg·L^{-1})	0.75	32.8	0.90	4.1	851.3	0.39	152.3	156.4	82.4	79.5
	1 mmol·L^{-1} KI	0.76	86.9	0.92	11.6	219.4	0.62	64.0	75.6	15.8	57.6
	5 mmol·L^{-1} KI	0.80	49.2	0.94	13.0	94.7	0.72	100.1	113.1	18.0	71.7
	TP + 1 mmol·L^{-1} KI	0.72	13.2	0.97	13.2	211.7	0.56	298.3	311.5	66.3	89.7
	TP + 5 mmol·L^{-1} KI	0.74	36.2	0.90	0.00	448.4	0.26	339.9	339.9	119.0	90.6

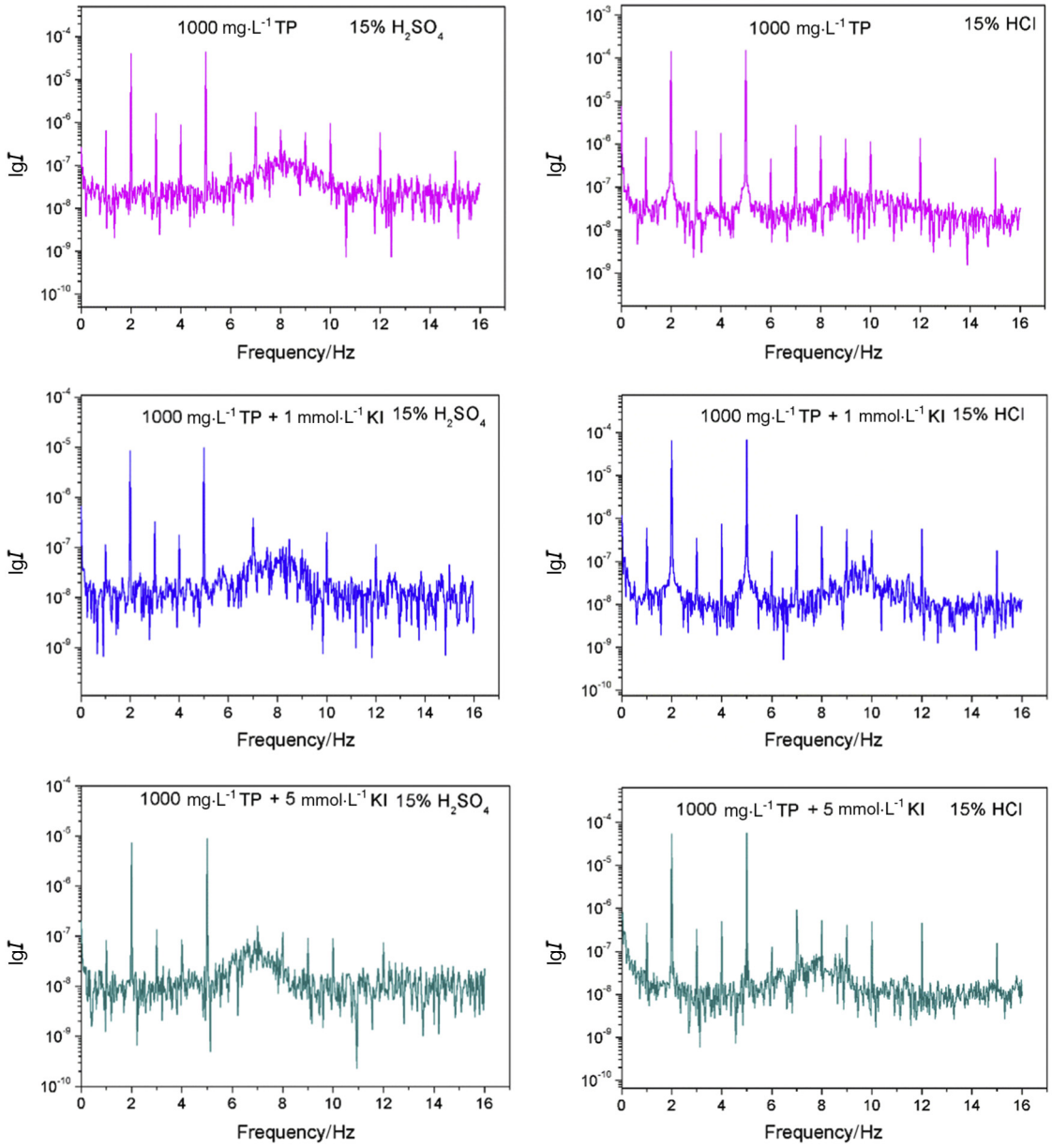

Fig. 9. Intermodulation spectrum recorded for St37 steel in 15% HCl solution in the absence and presence of TP (1000 mg·L^{-1}) and TP + KI mixtures at 25 °C.

Table 6
Electrochemical frequency modulation parameters for St37 steel in 15% HCl and 15% H_2SO_4 in the absence, presence of 1000 mg·L^{-1} TP, KI and TP + KI mixtures at 25 °C

Medium	Concentration	I_{corr}/μA·cm^{-2}	β_a/mV·dec^{-1}	β_c/mV·dec^{-1}	*CR*/mpy	*CF*-2	*CF*-3	*IE*/%
15% H_2SO_4	Blank	150.1	81.4	96.1	91.4	2.00	3.06	–
	TP (1000 mg·L^{-1})	62.7	87.0	110.7	38.2	1.45	2.98	58.2
	1 mmol·L^{-1} KI	18.4	89.5	112.8	11.2	2.44	2.74	87.7
	5 mmol·L^{-1} KI	15.4	89.61	100.2	9.4	2.08	2.65	89.7
	TP + 1 mmol·L^{-1} KI	16.5	103.6	137.8	10.1	1.89	3.50	89.0
	TP + 5 mmol·L^{-1} KI	13.6	102.9	116.2	8.3	1.68	2.79	90.9
15% HCl	Blank	928.0	95.9	105.7	533.7	1.69	3.13	–
	TP (1000 mg·L^{-1})	264.0	111.5	125.3	160.8	1.64	3.06	71.6
	1 mmol·L^{-1} KI	317.3	95.7	102.8	193.3	1.91	3.12	65.8
	5 mmol·L^{-1} KI	188.7	88.2	98.2	115.0	1.93	3.09	79.7
	TP + 1 mmol·L^{-1} KI	125.1	117.6	128.7	76.2	1.27	3.31	86.5
	TP + 5 mmol·L^{-1} KI	106.6	127.7	132.0	64.9	1.30	3.23	88.5

Table 7
Calculated values of the synergism parameter (S_1) from the various methods used

Inhibitor mixture	PDP	LPR	EIS	EFM
H_2SO_4				
TP + 1 mmol·L^{-1} KI	1.48	1.65	1.63	1.65
TP + 5 mmol·L^{-1} KI	1.46	1.65	1.65	1.63
HCl				
TP + 1 mmol·L^{-1} KI	1.58	1.51	1.53	1.60
TP + 5 mmol·L^{-1} KI	1.68	1.65	1.68	1.72

Table 8
Langmuir adsorption parameters for St37 steel in 15% HCl and 15% H_2SO_4 containing TP from different experimental methods at 25 °C

Corrosive medium	Experimental methods	ΔG^o_{ads}/kJ·mol^{-1}	$K_{ads} \times 10^2$/L·g^{-1}	Slope	R^2
15% H_2SO_4	LPR	−24.30	1.82	1.52	0.998
	EIS	−24.37	1.87	1.59	0.996
	EFM	−22.82	1.00	1.64	0.998
15% HCl	LPR	−24.39	1.89	1.24	0.998
	EIS	−24.54	2.00	1.21	0.999
	EFM	−26.36	4.18	1.37	0.998

iodide ions and organic inhibitors can co-adsorb on a metal surface in two ways; competitive or cooperative [26,27]. In competitive co-adsorption, iodide ions and organic cations adsorb on different sites in the metal surface [26] whereas in cooperative co-adsorption, the iodide ions first chemisorb on the metal surface and the organic cations adsorb on iodide ions adsorbed layer [26]. Competitive co-adsorption leads to antagonistic effect while cooperative co-adsorption gives rise to synergistic effect [26,28]. These two forms of co-adsorption can be differentiated using the synergism parameter. A value of $S_1 < 1$ signifies antagonistic effect while $S_1 > 1$ points to synergistic effect [26–28]. The synergism parameter can be calculated using the following equation [26,29]:

$$S_1 = \frac{1-(IE_1 + IE_2)}{1-IE_{1+2}} \quad (4)$$

where IE_1 is the inhibition efficiency of iodide ions, IE_2 is the inhibition efficiency of the inhibitor, IE_{1+2} is the inhibition efficiency of inhibitor + iodide ions. In our case, the calculated S_1 values (Table 7) are all greater than unity hence we conclude that the observed improvement on the corrosion inhibition efficiency of TP by iodide ions is due to synergistic effect.

3.4. Adsorption isotherm consideration

The use of adsorption isotherm to probe the adsorption characteristics of organic inhibitors is still a valid model [30–32]. The adsorption of organic inhibitor on metal surface depends on the degree of surface coverage (θ) [30]. The degree of surface coverage (θ) at different concentrations of TP on the St37 steel surface was calculated from the *IE* values ($\theta = IE/100$) obtained from LPR, EIS, and EFM experiments (Tables 1–3). By virtue of the linear regression coefficient (R^2) value which was approximately 1 in all cases (Table 8), the Langmuir

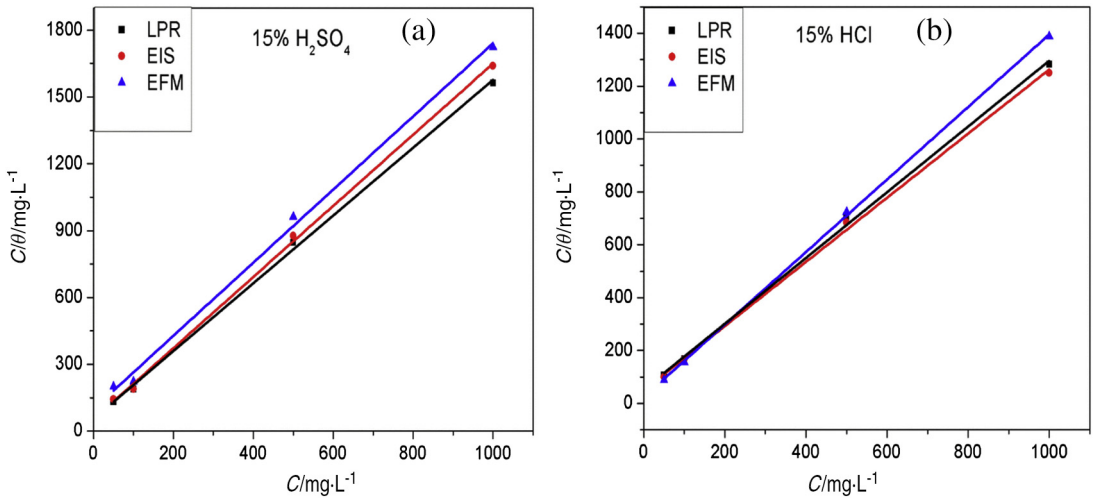

Fig. 10. Langmuir adsorption isotherm for St37 steel in (a) 15% H_2SO_4 and (b) 15% HCl containing TP from different experimental techniques.

adsorption isotherm was selected as the best fit isotherm for the studied systems. It has the general form:

$$\frac{C_{inh}}{\theta} = \frac{1}{K_{ads}} + C_{inh} \quad (5)$$

where C_{inh} is the inhibitor concentration and K_{ads} is the equilibrium constant for adsorption–desorption process [14]. The linear relationship for TP adsorption onto St37 steel surface obtained by plotting C_{inh}/θ *versus* C_{inh} is shown in Fig. 10.

As should be expected, the slopes of the graphs (Table 8) slightly deviated from unity required by an ideal Langmuir model indicating the existence of interaction in the adsorbed layer. Langmuir adsorption equation had been derived on the assumption that adsorbed molecules do not interact with each other [7]. This is not true as authors [7,23,33] have demonstrated that macromolecules like TP in adsorbed layer are capable of interaction. The K_{ads} value was computed from the intercepts of the graphs in Fig. 10 and as could be seen in Table 8, the value is low (*i.e.* between $(1.00–4.18) \times 10^{-2}\ L \cdot g^{-1}$) demonstrating low proportion of TP adsorbed on the St37 steel surface [14,34,35]. It also suggests less adherence of the TP adsorbed films on the metal surface. The higher the K_{ads} value, the tighter the adsorbed inhibitor film on the metal surface and the better the inhibitive ability [31]. To obtain information on the spontaneity of the adsorption process, the adsorption free energy

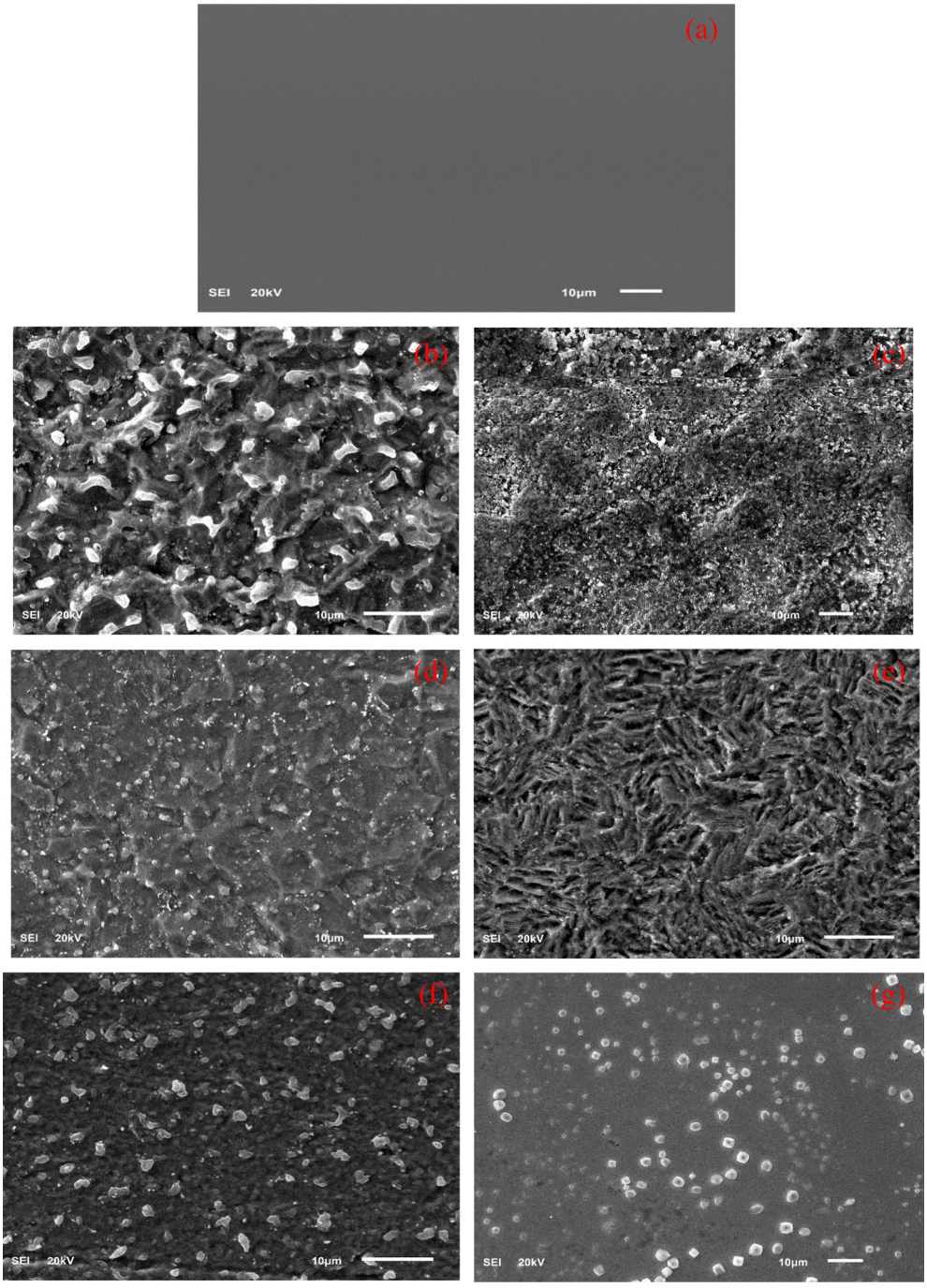

Fig. 11. SEM micrographs for St37 steel (a) in the polished state (b) exposed to 15% HCl, (c) exposed to 15% H_2SO_4, (d) exposed to 15% HCl containing 1000 $mg \cdot L^{-1}$ TP, (e) exposed to 15% H_2SO_4 containing 1000 $mg \cdot L^{-1}$ TP, (f) exposed to 15% HCl containing 1000 $mg \cdot L^{-1}$ TP + 5 $mmol \cdot L^{-1}$ KI and (d) exposed to 15% H_2SO_4 containing 1000 $mg \cdot L^{-1}$ TP + 5 $mmol \cdot L^{-1}$ KI after 24 h.

(ΔG^0_{ads}) was computed making use of the K_{ads} value according to the following equation [31,36]:

$$K_{ads} = \frac{1}{C_{water}} \exp\left(\frac{-\Delta G^0_{ads}}{RT}\right) \quad (6)$$

where C_{water} is the water concentration in the solution = 1000 g·L^{-1}, R is the molar gas constant, and T is the absolute temperature. The calculated ΔG^0_{ads} value from the various experimental methods are also given in Table 8. The value is negative and is indicative of spontaneous adsorption of TP molecules and stability on the St37 steel surface in the studied corrosive media [13,37].

3.5. Surface analysis

Fig. 11 shows the surface morphologies of St37 steel samples (a) before and after immersion in (b) 15% HCl solution, (c) 15% H_2SO_4 solution, (d) 15% HCl + 1000 mg·L^{-1} TP, (e) 15% H_2SO_4 + 1000 mg·L^{-1} TP, (f) 15% HCl + 1000 mg·L^{-1} TP + 5 mmol·L^{-1} KI, and (g) 15% H_2SO_4 + 1000 mg·L^{-1} TP + 5 mmol·L^{-1} KI solution for 24 h at 25 °C. Apparently, the smooth morphology of the specimens (Fig. 11(a)) is completely lost to corrosion upon exposure to the acid solutions. The surfaces thereafter exhibit rough and hilly-shaped morphologies (Fig. 11(b & c)). Compared with the surface in Fig. 11(c), the one in Fig. 11(b) is rougher inferring that St37 steel sample deteriorated in 15% HCl solution than in 15% H_2SO_4 solution. Undoubtedly, the metal samples were protected against corrosion in the acid solutions containing TP as evidenced in the relatively smoother surfaces in Fig. 11(d & e) compared to the ones in Fig. 11(b & c). It was deduced from experimental results (Tables 1–3) that TP retarded St37 steel dissolution in HCl medium than in H_2SO_4 environment. With a smoother surface morphology as observed in Fig. 11(d) than in Fig. 11(e), the surface analysis results agree with the experimental results. Again, it is obvious that addition of KI to TP enhanced the corrosion inhibition efficiency of TP in the acid environments and the effect is higher in H_2SO_4 environment than in HCl medium. Clearly, the image in Fig. 11(g) presents smoother morphology than the one in Fig. 11(f) but the surfaces in Fig. 11(d & e) are rougher than the surfaces in Fig. 11(f & g). Based on the experimental and surface analysis results, it is concluded that TP + KI combination offers a good corrosion protection to St37 steel in strong acid environments.

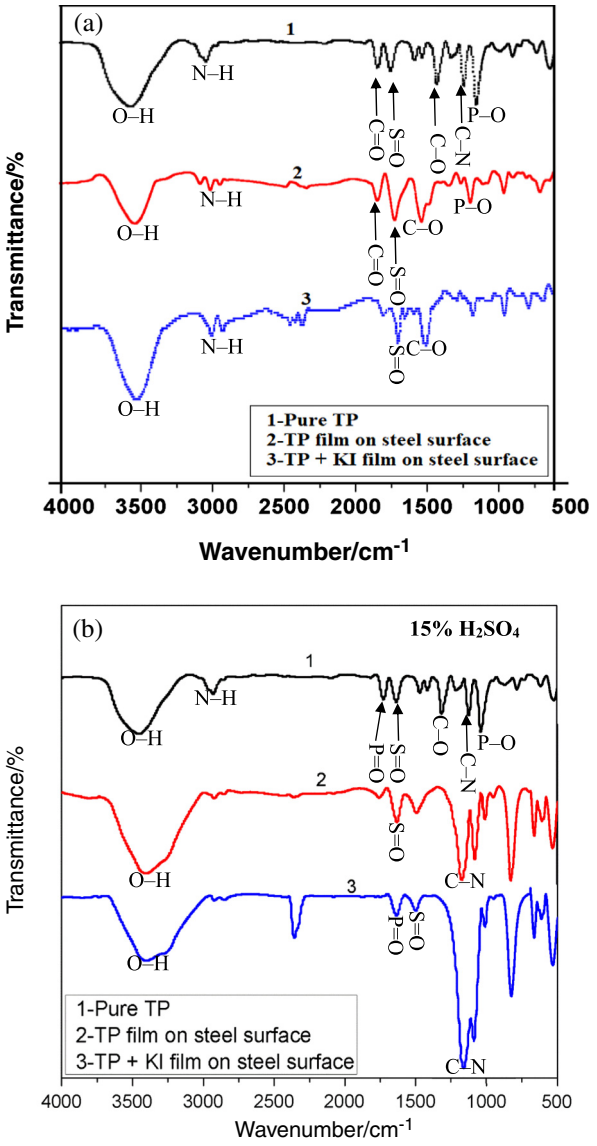

Fig. 12. FTIR spectra of pure TP, and film extracted from St37 surface immersed in (a) 15% HCl and (b) 15% H_2SO_4 containing TP and TP + KI mixtures.

3.6. Mechanism of corrosion inhibition

Inhibitors in acid solution can interact with metals and affect the corrosion reaction in a number of ways, some of which may occur simultaneously. It is practically impossible to assign a single general mechanism of action to an inhibitor because the mechanism may change with experimental conditions. Thus, the predominant mechanism of action of an inhibitor may vary with factors such as its concentration, the pH of the acid, the nature of the anion of the acid, the presence of other species in the solution, the extent of reaction to form secondary inhibitors, and the nature of the metal [30,38,39]. Our experimental results reveal that TP inhibits St37 steel corrosion better in HCl solution than H_2SO_4 solution but TP + KI mixture is a better inhibitor in H_2SO_4 than HCl solution. Generally, metal corrosion inhibition by adsorption mechanism is a quasi-substitution process and could be by physisorption or chemisorption [40,41]. TP in the strong acids could be protonated and there is every tendency that St37 steel surface acquires net positive charge. Adsorption of protonated forms of TP onto charged St37 steel surface would be greatly influenced by the anions present in the solution. As it is known, in HCl solution, chloride ions are specifically adsorbed on metal surface while sulphate ions are adsorbed in H_2SO_4 medium [26,28]. The chloride ions have a higher shielding power than the sulphate ions therefore more of protonated TP should be expected to adsorbed on the St37 steel surface recharged by chloride ions than one recharged by sulphate ions. Nevertheless, adsorbed protonated molecules could be deprotonated and the freed heteroatoms go into coordinate type of bond with metal surface [12,42]. Such complex formation would lead to better corrosion protection [12,42]. To gain insight into the corrosion inhibition of St37 steel in HCl and H_2SO_4 media by TP and TP + KI and to explain why TP + KI better inhibits in H_2SO_4 solution than HCl, FTIR and UV–vis experiments were undertaken. Fig. 12 shows the FTIR spectra of pure TP, TP film, and TP + KI film extracted from St37 steel surface after immersion in (a) HCl solution and (b) H_2SO_4 medium. The spectrum of the pure TP is characterized with peaks at 3500 cm^{-1}, 3100 cm^{-1}, 1850 cm^{-1}, 1613.2 cm^{-1}, 1320 cm^{-1}, 1282 cm^{-1}, and 1000 cm^{-1}. They correspond to O—H [7,11], N—H [43], C═O [15], S═O [44], C—O [45], C—N [46], and P—O [45] stretching vibrations respectively. Compared with the TP and TP + KI film spectra in Fig. 12(a), the P—O and S═O peaks shifted to 1100 cm^{-1} and 1702 cm^{-1} respectively and are more intense, the C—O, C═O, and N—H peaks diminish and are less intense. In Fig. 12(b), the N—H peak almost completely disappear while the C—O peak becomes more intense in the TP and TP + KI spectra compared to the pure TP. All these reflect the involvement of the

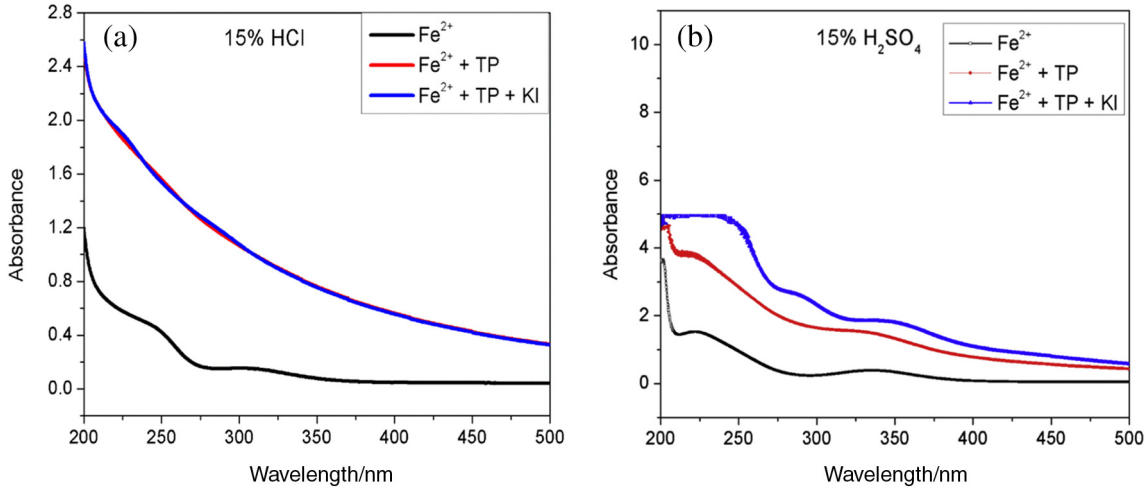

Fig. 13. UV–Vis spectra of (a) 15% HCl and (b) 15% H_2SO_4 solutions without and with 1000 mg·L^{-1} TP and 1000 mg·L^{-1} TP + KI mixtures after St37 steel immersion for 24 h at 25 °C.

heteroatoms in the adsorption process. However, the adsorption mechanism seems to be different for TP and TP + KI in HCl and H_2SO_4 solutions. For instance, the N—H peak is almost absent in the TP and TP + KI spectra in Fig. 12(b) but not so in Fig. 12(a). Also, the C—O peak is stronger in the TP and TP + KI spectra in Fig. 12(b) than in Fig. 12(a) and new peak emerged in the TP + KI spectrum at 2500 cm^{-1} in Fig. 12(b). The UV–vis spectra presented in Fig. 13 give a clearer picture to the adsorption processes in the studied systems. The solutions resulting from St37 steel immersion in the acid solutions yielded spectra with two bands, one at 250 nm and the other at 300 nm, while the spectra for 15% HCl containing the additives shows no band. This means that, in the presence of both TP and TP + KI, there was no complex formation. The adsorbed inhibitor films were held on the metal surface by electrostatic force. The non-formation or formation of unstable Fe-inhibitor complex even in the presence of iodide ions in the HCl solution may have been caused by competitive adsorption between Cl^- and I^- ions. As it is known, in HCl environment, the specific adsorption of chloride ions is on the anodic site while hydronium ions are adsorbed at the cathodic site [39,47,48]. Our PDP results (Fig. 7(a)) clearly shows that in HCl solution, addition of KI did not affect the anodic reactions but affected only the cathodic reactions. It means that there was some sort of opposition from chloride ions to iodide ions on the anodic site and this may have resulted in formation of unstable or non-formation of complex at all. In the Fe^{2+} + TP + KI spectrum of Fig. 13(b), three clear bands at 250 nm, 300 nm, and 350 nm can be identified. The appearance of the new peak at 350 nm justify the formation of Fe-inhibitor complex. Similar submission can be found in the corrosion literature [15]. This new band corresponds to the extra peak at 2500 cm^{-1} in Fig. 12(b). The complex so formed in H_2SO_4 solution ensured better corrosion mitigation than in HCl solution. It should also be mentioned that iodide ions suffered less opposition in H_2SO_4 solution as evidenced in the PDP result in Fig. 7(b); both the anodic and cathodic reactions are affected by KI addition.

4. Conclusions

A novel tetrapolymer (TP) consisting of carboxylate, sulphonate, phosphonate and sulfur dioxide based co-monomers has been successfully synthesized using Butler cyclopolymerization technique and characterized using FTIR, ^{1}H-NMR, ^{13}C NMR and elemental analysis. The tetrapolymer is a moderate corrosion inhibitor for St37 steel in 15% HCl and 15% H_2SO_4 acid media but better in HCl medium than in H_2SO_4 solution. Addition of small amount of KI to the tetrapolymer synergistically enhanced TP corrosion inhibition efficiency. 5 mmol·L^{-1} KI upgraded TP corrosion inhibition efficiency from 61.1% and 79.5% in H_2SO_4 and HCl solutions respectively to 93.5% and 90.6% according to the EIS results. TP and TP + KI afforded the corrosion inhibition of St37 steel in the acid media by virtue of adsorption mechanism according to ATR-FTIR analysis results and the adsorption process followed Langmuir adsorption isotherm. TP + KI formed complex with St37 steel surface in H_2SO_4 solution but not in HCl solution.

Acknowledgements

The authors gratefully acknowledged the financial support provided by Imam Abdulrahman Bin Faisal University (IAU) through project number: 2016-237-Eng. Some research facilities were provided by the Centre of Research Excellence in Corrosion; KFUPM is thankfully acknowledged.

References

[1] P. Rajeev, A.O. Surendranathan, Ch.S.N. Murthy, Corrosion mitigation of the oil well steels using organic inhibitors — A review, *J. Mater. Environ. Sci.* 3 (5) (2012) 856–869.
[2] A. Biswas, S. Pal, G. Udayabhanu, Experimental and theoretical studies of xanthan gum and its graft co-polymer as corrosion inhibitor for mild steel in 15% HCl, *Appl. Surf. Sci.* 353 (2015) 173–183.
[3] M.M. Solomon, S.A. Umoren, In-situ preparation, characterization and anticorrosion property of polypropylene glycol/silver nanoparticles composite for mild steel corrosion in acid solution, *J. Colloid Interface Sci.* 462 (2016) 29–41.
[4] M.M. Solomon, H. Gerengi, S.A. Umoren, N.B. Essien, U.B. Essien, E. Kaya, Gum Arabic-silver nanoparticles composite as a green anticorrosive formulation for steel corrosion in strong acid media, *Carbohydr. Polym.* 181 (2018) 43–55.
[5] M.M. Solomon, H. Gerengi, T. Kaya, S.A. Umoren, Enhanced corrosion inhibition effect of chitosan for St37 in 15% H_2SO_4 environment by silver nanoparticles, *Int. J. Biol. Macromol.* 104 (2017) 638–649.
[6] H.H.H. Hefni, E.M. Azzam, E.A. Badr, M. Hussein, S.M. Tawfik, Synthesis, characterization and anticorrosion potentials of chitosan-g-PEG assembled on silver nanoparticles, *Int. J. Biol. Macromol.* 83 (2016) 297–305.
[7] M.M. Solomon, H. Gerengi, S.A. Umoren, Carboxymethyl cellulose/silver nanoparticles composite: Synthesis, characterization and application as a benign corrosion Inhibitor for St37 steel in 15% H_2SO_4 medium, *ACS Appl. Mater. Interfaces* 9 (2017) 6376–6389.
[8] S.A. Haladu, S.A. Umoren, S.A. Ali, M.M. Solomon, synthesis and characterization of cyclic cationic polymer and its anti-corrosion property for low carbon steel in 15% HCl solution, *Int. J. Electrochem. Sci.* 12 (2017) 9061–9083.
[9] S.A. Umoren, Polypropylene glycol: A novel corrosion inhibitor for ×60 pipeline steel in 15% HCl solution, *J. Mol. Liq.* 219 (2016) 946–958.
[10] S.A. Ali, S.A. Haladu, M.A.J. Mazumder, H.A. Al-Muallem, Synthesis of a terpolymer and a tetrapolymer using monomers of diallylamine salts and SO_2 and their application as antiscalants, *Iran. Polym. J.* 25 (2016) 747–756.
[11] M.M. Solomon, H. Gerengi, T. Kaya, S.A. Umoren, Performance evaluation of chitosan/silver nanoparticles composite on St37 steel corrosion in 15% HCl solution, *ACS Sustain. Chem. Eng.* 5 (1) (2017) 809–820.

[12] H. Gerengi, I. Uygur, M. Solomon, M. Yildiz, H. Goksu, Evaluation of the inhibitive effect of *Diospyros kaki* (persimmon) leaves extract on St37 steel corrosion in acid medium, *Sustain. Chem. Pharm.* 4 (2016) 57–66.
[13] P. Han, C. Chen, W. Li, H. Yu, Y. Xu, L. Ma, Y. Zheng, Synergistic effect of mixing cationic and nonionic surfactants on corrosion inhibition of mild steel in HCl: Experimental and theoretical investigations, *J. Colloid Interface Sci.* 516 (2018) 398–406.
[14] G. Sığırcık, T. Tüken, M. Erbil, Assessment of the inhibition efficiency of 3,4-diaminobenzonitrile against the corrosion of steel, *Corros. Sci.* 102 (2016) 437–445.
[15] P.E. Alvarez, M.V. Fiori-Bimbi, A. Neske, S.A. Brandán, C.A. Gervasi, *Rollinia occidentalis* extract as green corrosion inhibitor for carbon steel in HCl solution, *J. Ind. Eng. Chem.* 58 (2018) 92–99.
[16] M. Abdallah, H. MAl-Tass, B.A. AL Jahdaly, A.S. Fouda, Inhibition properties and adsorption behavior of 5-arylazothiazole derivatives on 1018 carbon steel in 0.5 M H_2SO_4 solution, *J. Mol. Liq.* 216 (2016) 590–597.
[17] J. Pan, D. Thierry, C. Leygraf, Electrochemical impedance spectroscopy study of the passive oxide film on titanium for implant application, *Electrochim. Acta* 41 (1996) 1143–1153.
[18] Z.B. Wang, H.X. Hu, Y.G. Zheng, W. Ke, Y.X. Qiao, Comparison of the corrosion behavior of pure titanium and its alloys in fluoride-containing sulfuric acid, *Corros. Sci.* 103 (2016) 50–65.
[19] Z.B. Wang, H.X. Hu, Y.G. Zheng, Synergistic effects of fluoride and chloride on general corrosion behavior of AISI 316 stainless steel and pure titanium in H_2SO_4 solutions, *Corros. Sci.* 130 (2018) 203–217.
[20] S.S. Abdel-Rehim, K.F. Khaled, N.S. Abd-Elshafi, Electrochemical frequency modulation as a new technique for monitoring corrosion inhibition of iron in acid media by new thiourea derivative, *Electrochim. Acta* 51 (2006) 3269–3277.
[21] I.B. Obot, I.B. Onyeachu, Electrochemical frequency modulation (EFM) technique: Theory and recent practical applications in corrosion research, *J. Mol. Liq.* 249 (2018) 83–96.
[22] M.M. Solomon, S.A. Umoren, Electrochemical and gravimetric measurements of inhibition of aluminum corrosion by poly (methacrylic acid) in H_2SO_4 solution and synergistic effect of iodide ions, *Measurement* 76 (2015) 104–116.
[23] S.A. Umoren, M.M. Solomon, I.I. Udosoro, A.P. Udoh, Synergistic and antagonistic effects between halide ions and carboxymethyl cellulose for the corrosion inhibition of mild steel in sulphuric acid solution, *Cellulose* 17 (2010) 635–648.
[24] M.M. Solomon, H. Gerengi, T. Kaya, E. Kaya, S.A. Umoren, Synergistic inhibition of St37 steel corrosion in 15% H_2SO_4 solution by chitosan and iodide ion additives, *Cellulose* 24 (2017) 931–950.
[25] B. Qian, J. Wang, M. Zheng, B. Hou, Synergistic effect of polyaspartic acid and iodide ion on corrosion inhibition of mild steel in H_2SO_4, *Corros. Sci.* 75 (2013) 184–192.
[26] A.A. Farag, M.A. Hegazy, Synergistic inhibition effect of potassium iodide and novel Schiff bases on X65 steel corrosion in 0.5 M H_2SO_4, *Corros. Sci.* 74 (2013) 168–177.
[27] D.-Q. Zhang, L.-X. Gao, G.-D. Zhou, Synergistic effect of 2- mercaptobenzimidazole and KI on copper corrosion inhibition in aerated sulfuric acid solution, *J. Appl. Electrochem.* 33 (2003) 361–366.
[28] A.Y. Musa, A.B. Mohamad, A.A.H. Kadhum, M.S. Takriff, L.T. Tien, Synergistic effect of potassium iodide with phthalazone on the corrosion inhibition of mild steel in 1.0 M HCl, *Corros. Sci.* 53 (2011) 3672–3677.
[29] L. Larabi, Y. Harek, M. Traisnel, A. Mansri, Synergistic influence of poly(4-vinylpyridine) and potassium iodide on inhibition of corrosion of mild steel in 1 M HCl, *J. Appl. Electrochem.* 34 (2004) 833–839.
[30] A.O. Yüce, E. Telli, B.D. Mert, G. Kardaş, B. Yazıcı, Experimental and quantum chemical studies on corrosion inhibition effect of 5,5 diphenyl 2-thiohydantoin on mild steel in HCl solution, *J. Mol. Liq.* 218 (2016) 384–392.
[31] Y. Qiang, S. Zhang, B. Tan, S. Chen, Evaluation of Ginkgo leaf extract as an eco-friendly corrosion inhibitor of X70 steel in HCl solution, *Corros. Sci.* 133 (2018) 6–16.
[32] Y. Hao, L.A. Sani, T. Ge, Q. Fang, The synergistic inhibition behaviour of tannic acid and iodide ions on mild steel in H_2SO_4 solutions, *Corros. Sci.* 123 (2017) 158–169.
[33] Z. Tao, W. He, S. Wang, S. Zhang, G. Zhou, A study of differential polarization curves and thermodynamic properties for mild steel in acidic solution with nitrophenyltriazole derivative, *Corros. Sci.* 60 (2012) 205–213.
[34] X. Zhou, H. Yang, F. Wang, [BMIM]BF4ionic liquids as effective inhibitor forcarbon steel in alkaline chloride solution, *Electrochim. Acta* 56 (2011) 4268–4275.
[35] B. Xu, Y. Liu, X. Yin, W. Yang, Y. Chen, Experimental and theoretical study ofcorrosion inhibition of 3-pyridinecarbozalde thiosemicarbazone for mild steelin hydrochloric acid, *Corros. Sci.* 74 (2013) 206–213.
[36] N. El Hamdani, R. Fdil, M. Tourabi, C. Jama, F. Bentiss, Alkaloids extract of *Retama monosperma* (L.) Boiss. seeds used as novel eco-friendly inhibitor for carbon steel corrosion in 1M HCl solution: electrochemical and surface studies, *Appl. Surf. Sci.* 357 (2015) 1294–1305.
[37] D.B. Hmamou, R. Salghi, A. Zarrouk, H. Zarrok, R. Touzani, B. Hammouti, A. El Assyry, Investigation of corrosion inhibition of carbon steel in 0.5 M H2SO4 by new bipyrazole derivative using experimental and theoretical approaches, *J. Environ. Chem. Eng.* 3 (2015) 2031–2041.
[38] D.P. Schweinsberg, V. Ashworth, The inhibition of the corrosion of pure iron in 0.5 M sulphuric acid by n-alkyl quaternary ammonium iodides, *Corros. Sci.* 28 (1988) 539–545.
[39] M. Yildiz, H. Gerengi, M.M. Solomon, E. Kaya, S.A. Umoren, Influence of 1-butyl-1-methylpiperidinium tetrafluoroborate on St37 steel dissolution behavior in HCl environment, *Chem. Eng. Commun.* 205 (4) (2018) 538–548.
[40] M. Heydari, M. Javidi, Corrosion inhibition and adsorption behaviour of an amido-imidazoline derivative on API 5L X52 steel in CO_2-saturated solution and synergistic effect of iodide ions, *Corros. Sci.* 61 (2012) 148–155.
[41] I.B. Obot, Synergistic effect of nizoral and iodide ions on the corrosion inhibition of mild steel in sulphuric acid solution, *Port. Electrochim. Acta* 27 (2009) 539–553.
[42] X. Li, S. Deng, H. Fu, Triazolyl blue tetrazolium bromide as a novel corrosion inhibitor for steel in HCl and H_2SO_4 solutions, *Corros. Sci.* 53 (2011) 302–309.
[43] M.F. Zayed, W.H. Eisa, Y.K. Abdel-Moneam, S.M. El-Kousy, *Ziziphus spina-christi* based bio-synthesis of Ag nanoparticles, *J. Ind. Eng. Chem.* 23 (2015) 50–56.
[44] V. Gopinath, D. Mubarakali, S. Priyadarshini, N. Meera Priyadharsshini, Biosynthesis of silver nanoparticles from *Tribulus terrestris* and its antimicrobial activity: a novel biological approach, *Colloids Surf. B: Biointerfaces* 96 (2012) 69–74.
[45] Y. Sasikumar, M.M. Solomon, L.O. Olasunkanmi, E.E. Ebenso, Effect of surface treatment on the bioactivity and electrochemical behavior of magnesium alloys in simulated body fluid, *Mater. Corros.* 68 (2017) 776–790.
[46] M. Nasrollahzadeh, S.M. Sajadi, F. Babaei, M. Maham, *Euphorbia helioscopia Linn* as a green source for synthesis of silver nanoparticles and their optical and catalytic properties, *J. Colloid Interface Sci.* 450 (2015) 374–380.
[47] M. Kowsari, R. Payami, B. Amini, M. Ramezanzadeh, E. Javanbakh, Task-specific ionic liquid as a new green inhibitor of mild steel corrosion, *Appl. Surf. Sci.* 289 (2014) 478–486.
[48] N.V. Likhanova, M.A. Dominguez-Aguilar, O. Olivares-Xometl, N. Nava-Entzana, E. Arce, H. Dorantes, The effect of ionic liquids with imidazolium and pyridinium cations on the corrosion inhibition of mild steel in acidic environment, *Corros. Sci.* 52 (2010) 2088–2097.